Available online at www.sciencedirect.com
ScienceDirect
Journal of Photochemistry and Photobiology A: Chemistry 190 (2007) 258–273
Journal of Photochemistry and Photobiology A:Chemistry
www.elsevier.com/locate/jphotochem

# Substituent-controlled photoisomerization in retinal chromophore models: Fluorinated and methoxy-substituted protonated Schiff bases☆

Irene Conti, Marco Garavelli *

*Dipartimento di Chimica 'G. Ciamician', Via Selmi 2, 40126 Bologna, Italy*

Available online 6 December 2006

**Abstract**

The effect of substitution on the intrinsic (i.e. *in vacuo*) photoisomerization ability of retinal chromophore models has been explored using CASPT2//CASSCF minimum energy path computations to map the $S_1$ photoisomerization paths of two substituted minimal models of the retinal chromophore: the 2-*cis*-penta-2,4-dieniminium and the all-*trans*-epta-2,4,6-trieniminium cations, which have been modified using fluorine or methoxyl substituents as representative examples of electron-withdrawing and electron-releasing groups, respectively. A systematic analysis has been performed involving substitutions in all the possible positions along the chain. It is shown that the photochemical reactivity and photoisomerization efficiency of these systems may be tuned or indeed changed, although this effect strongly depends on the position of the substituent. In particular, we have shown that (i) most of the systems preserves qualitatively the reactivity of the parent (i.e. unsubstituted) compound; (ii) substitution at positions C4 or C6 leads to a different relaxed excited state structure of the chromophore and in general to a very flat photoisomerization path (or to a tiny $S_1$ energy barrier in some cases); (iii) the nature of the TICT state (i.e. the $S_1 \rightarrow S_0$ decay funnel) may be turned from a conical intersection into an excited state minimum; (iv) for the C4 methoxy-substituted system the isomerization path as well as the $S_1/S_0$ decay funnel involve an unusual torsional angle. Thus, substitution turns out to be a good tool not only to tune the optical properties (i.e. the absorption and emission features) of the chromophore (as we have already shown in a previous work: I. Conti, F. Bernardi, G. Orlandi, M. Garavelli, Mol. Phys. 104 (2006) 915–924), but it may also play a crucial role in tuning and controlling photoisomerization selectivity and efficiency, affecting excited state lifetime and reaction rate. A rationale for these effects is presented, which provides a basis for understanding reactivity properties and the *intrinsic* photochemical behavior of substituted retinal chromophores.


*Keywords:* Conical intersections; Photoisomerization; Retinal; CASPT2//CASSCF; Substitution

## 1. Introduction

Rhodopsin proteins [1–10] exploit the ability of their chromophore to efficiently transduce radiative energy into chemical (i.e. kinetic) energy. For this purpose, an ultrafast (i.e. subpicosecond) and efficient (i.e. ca. 70% quantum yield) light-induced *cis–trans* isomerization of the chromophore (a retinal which is covalently linked to the protein via a protonated Schiff base (PSB) linkage) takes place, which triggers the biological activity of the photoreceptor and is often referred to as the primary photochemical event. The retina visual pigment rhodopsin (Rh) and the bacterial proton pump bacteriorhodopsin (bR) (whose chromophores correspond to the 11-*cis* (PSB11) and all-*trans* (PSBT) stereoisomers of the PSB of retinal, respectively) are among the most studied examples of this kind.

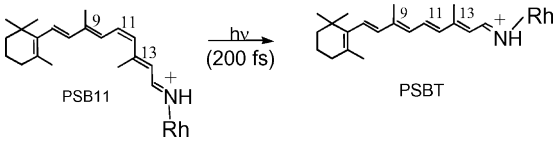


(1)

Results of *ab initio* CASPT2//CASSCF minimum energy path (MEP) mapping for the photoisomerization *in vacuo* of reduced models of the retinal chromophore have been recently reported [11–17]. These include, among the others, the PSB11 model 4-*cis*-γ-methylnona-2,4,6,8-tetraeniminium cation [12,16,17] and the minimal PSB11 and PSBT models 2-*cis*-penta-2,4-dieniminium [18] and all-*trans*-hepta-2,4,6-

*Abbreviations:* MEP, minumum energy path; PES, potential energy surface; CI, conical intersection; PSB, protonated Schiff base; PSB11, 11-*cis* Retinal protonated Schiff base; PSBT, all-*trans* Retinal protonated Schiff base; OBF, one-bond-flip; IRD, initial-relaxation-direction

☆ Published in the journal website (www.ASPjournal.com) on 11 January 2007.

* Corresponding author. Tel.: +39 051 2099476; fax: +39 051 2099456.
*E-mail address:* marco.garavelli@unibo.it (M. Garavelli).

1010-6030/$ – see front matter © 2007 Elsevier B.V. All rights reserved.
doi:10.1016/j.jphotochem.2006.12.006

trieniminium [19] cations, respectively. These investigations have provided a unified and unambiguous (although qualitative) view of the *intrinsic* (i.e. absence of environmental effects) photochemical reactivity of PSB. Despite the different length of the conjugated chains (which quantitatively affects the spectroscopy and the energetic of the system) and the lack of the retinal β-ionone ring (which could play a role in the steric factors involved in constrained environments), it has been shown that the photochemical behavior of these systems is similar, the reaction mechanism being characterized by an efficient photoisomerization path on the spectroscopic (charge transfer) state $S_1$, which is essentially barrierless and drives the system into a peaked $S_1/S_0$ conical intersection (CI) funnel (i.e. the excited and ground states are degenerate) with a twisted central double bond. It has been shown that $S_1$ can be related to the $1B_u$ – i.e. hole-pair (ionic) – state of polyenes and that the $S_1/S_0$ conical intersection has the form of a twisted intramolecular charge transfer (TICT) state [12,16,17,20]: substantially, a net electron has been transferred from the **C**-terminal side (**tail**) to the **N**-terminal side (**head**) of the skeleton and, consequently, the positive charged has moved from the **head** to the **tail**. The corresponding $S_1$ isomerization coordinate, starting at a planar Franck Condon point (FC), is *bimodal* being sequentially dominated by two uncoupled modes. The first (describing relaxation out of the FC region) corresponds to a stretching mode involving C–C bonds order inversion and leads to a planar stationary point ($SP_{standard}$) possessing an inverted double-bond/single-bond alternation. The second mode (following right away after the first) breaks the planar symmetry and is dominated by a one-bond-flip (OBF) [21,22] twisting of the reacting double bond. These results qualitatively account for the ultrafast radiationless decay [23–26] and high photoisomerization quantum yield observed in retinal chromophores and, more in general, in PSBs [27].

A schematic illustration of the bimodal reaction coordinate is shown in Fig. 1, where the minimum energy paths computed for the all-*trans*-hepta-2,4,6-trieniminium cation [19] are reported together with a pictorial view of the structure of the $S_1$ energy surface. As shown in the figure, the path switches from the

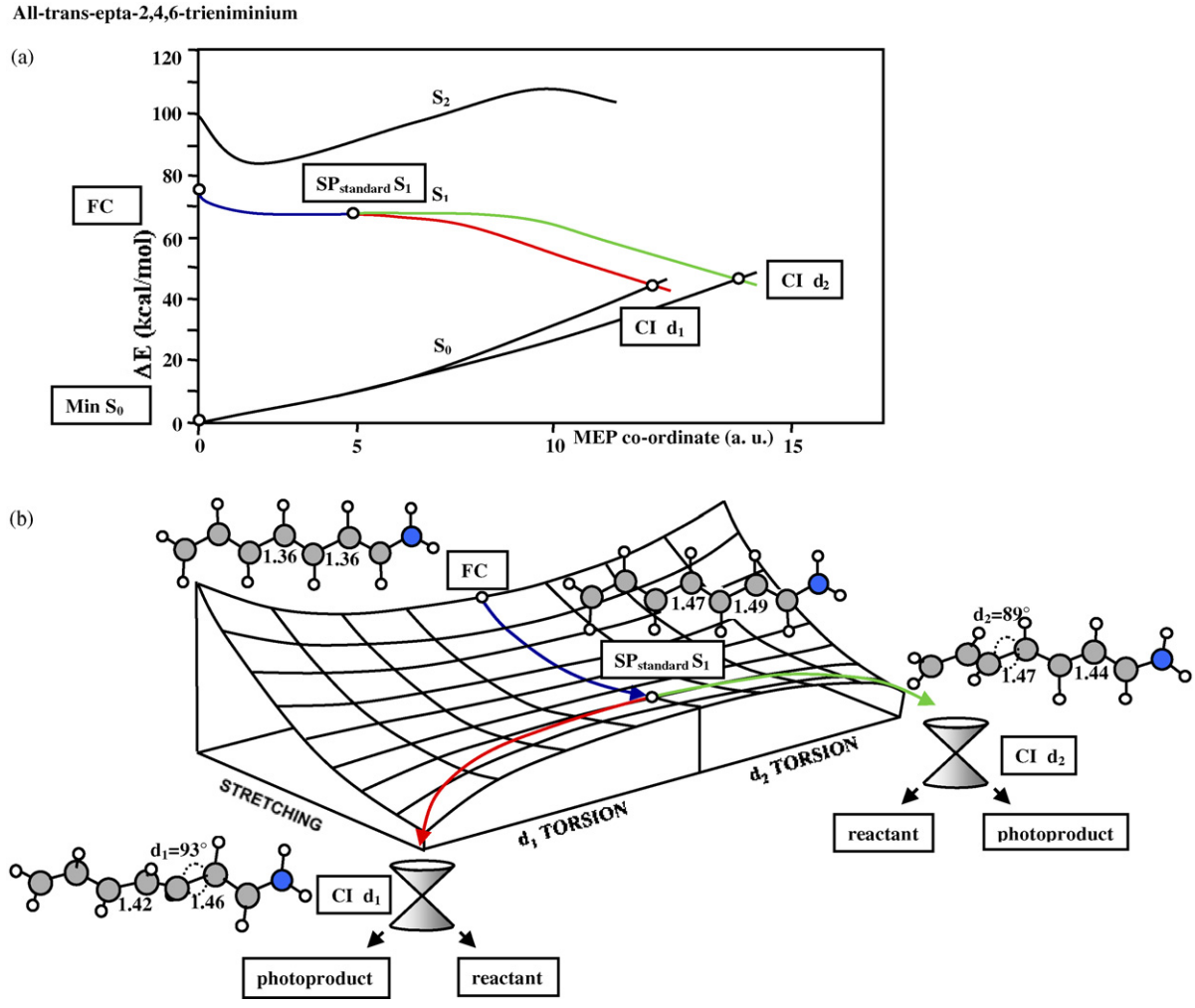


Fig. 1. (a) $S_0$, $S_1$ ($1B_U$-like) and $S_2$ ($2A_g$-like) energy profiles along the MEPs describing the two competing (red and green lines) $S_1$ isomerization paths from the Franck Condon point (FC) to the decay points (conical intersections) CI $d_1$ and CI $d_2$ of model **2**. The relaxed planar stationary point is labeled as $SP_{standard}$ $S_1$. (b) Schematic illustration of the starting stretching mode coordinate (blue line) and the orthogonal torsional reaction coordinate (red and green lines) along the MEP. The structures (geometrical parameters in Å and degrees) document the geometrical progression along the bimodal reaction path (for interpretation of the references to color in this figure legend, the reader is referred to the web version of the article).

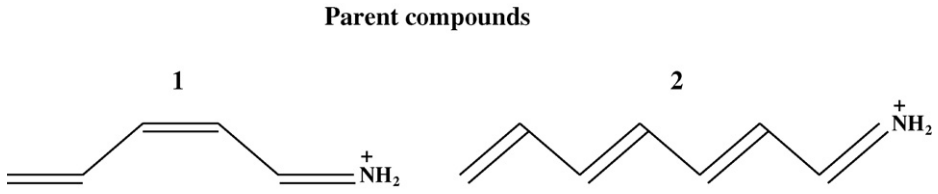


Scheme 1.

stretching to the torsional modes in the region of the planar stationary point (see the $SP_{standard}$ $S_1$ structure in Fig. 1) located at the center of a rather long energy plateau (note that two competing OBF processes exist each one involving the isomerization of one of the two internal double bonds).

Anyway, the isomerization paths mentioned above involve only bare and unsubstituted PSB models. Recently, to explore the effects of substitution in tuning the photochemical reactivity, we have reported the results of CASPT2//CASSCF photoisomerization and relaxation path computations for locked PSB models (i.e. the chromophore has been substituted with an alckylic *ring-lock* which restrains – fully or partially – the torsional deformation of the reactive double bond which is part of the cyclic moiety) [20]. Ring-size-dependent effects have been unveiled in these systems, which are in agreement with the experiments and provide a nice explanation for the observations recorded on artificial pigments containing synthetic *ring-locked* retinal chromophores: namely, the effects in the photoisomerization efficiency/selectivity and the decrease or increase in the excited state lifetime. Furthermore, the possibility of electrostatic tuning of the photochemical mechanism has been investigated by us [13,15] and more recently by other authors [28]. It has been shown that the location of the lowest energy deactivation funnel (which controls the photoisomerization stereoselectivity) depends on the position of an external countercharge and that this is to be expected on the basis of involvement of a charge transfer state $S_1$. Thus, it is suggested that an exogenous charge can be used as a tool to tune and control the photochemical process.

To provide further information about the intrinsic photochemical behavior of *substituted* retinal chromophores, in the present work we present the results of CASPT2//CASSCF excited state reaction path computations for fluorinated and methoxy-substituted retinal PSB models whose parent compounds have already been investigated in the past (and are considered here for comparison): the minimal PSB models 2-*cis*-penta-2,4-dieniminium (**1**) [18] and all-*trans*-epta-2,4,6-trieniminium (**2**) [19] cations (see Scheme 1). Fluorine and methoxyl have been chosen as prototypes of electron-withdrawing and electron-donating groups, respectively, and because retinal chromophores have been successfully synthesized with fluorine [29] and methoxyl [30] substituents in different positions along the chain. A systematic analysis of the position-dependent effects of these substituents on the photochemical reactivity has been performed and reported here, involving substitutions in different positions along the chain (see Scheme 2). This work complements a recently published report on the same substituted systems and provides its natural extension [31]: while there we focused on the change and tuning of the optical properties (i.e. absorption and emission features), here we investigate on their photochemical reactivity, thus presenting a full comprehensive picture of substituent effects on the photophysical and photochemical properties of PSBs.

Below we show that the effects of the substituent on the photochemical behavior of these systems is position-dependent and may be quite relevant. According to the computational results, it is anticipated that a tuning in the excited state lifetime and reaction rate, as well as a control in photoisomerization selectivity/efficiency, is expected. A simple interpretative model for the reactivity is provided, which allows an understanding of the simulated effects and should be of brad applicability in substituted PSB chromophores in general.

## 2. Computational methods

CASPT2//CASSCF/6-31G* fully unconstrained MEPs computations have been used to map the $S_1$ photoisomerization paths of the chosen models *in vacuo* and a description of the singlet manifold (i.e. the first three low-energy states $S_0$, $S_1$ and $S_2$) along these paths has been provided. Thus, consistently with previous works [12,16], excited state isomerization paths are

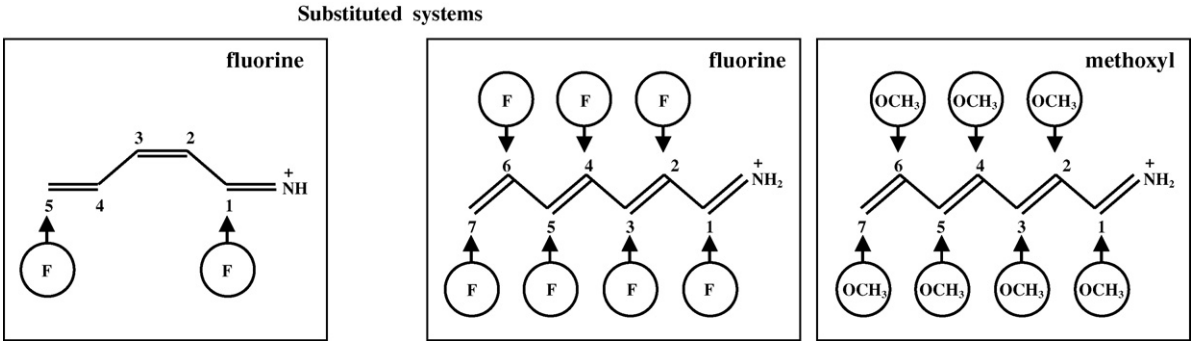


Scheme 2.

computed in terms of MEPs in mass-weighted coordinates, using the initial-relaxation-direction (IRD) methodology [32,33]. The CASPT2//CASSCF strategy requires that the reaction coordinate is computed at the complete active space self-consistent field (CASSCF) level and that the corresponding energy profile is re-evaluated on the multiconfigurational second-order Møller–Plesset perturbation theory level (here we used the CASPT2 method implemented in MOLCAS-5) [34] to take into account the effect of electron dynamic correlation and increase the accuracy of the paths energy profile.

The active space is selected to include the full polyenic π-system and the heteroatom p-lone pairs that may be involved in the conjugation. Therefore, an active space of 8 electrons in 7 orbitals has been used for fluorinated **1** (comprising the polyenic π-system and the p-electronic lone-pair on fluorine). Anyway, computations show that this lone-pair never gets involved in the description of the electronic wavefunction (i.e. it is always doubly occupied: note that this behavior demonstrates that fluorine effects on the reaction profiles do depend only in small part from mesomeric effects). Consequently, a reduced active space of 8 electrons in 8 orbitals (comprising only the polyenic π-system) has been used for fluorinated **2**, while a 10 π-electrons in 9 π-orbitals active space has been selected in methoxy-substituted **2** (i.e. including the p-electronic lone-pair on oxygen). (An active space of 12 electrons in 10 orbitals was initially selected for methoxy-substituted **2**, which included also the oxygen lone-pair *n* to account for possible low-lying $n \rightarrow p^*$ excited states. Anyway, $n \rightarrow \pi^*$ excited states appeared to be too far higher in energy to get involved in the photochemistry of the system. Therefore, all the computations have been performed with the reduced active space by taking out the lone-pair *n*.)

All geometry optimizations and relaxation paths mapping were carried out using the tools available in the GAUSSIAN98 suite of programs [35]. Both single-state and state-average (with equal weights among all roots) CASSCF energy calculations have been performed, depending by the specific situation encountered as specified throughout the text. As stated before, energies of stationary points, CIs and selected points along the MEPs have been re-evaluated using single point calculations performed at the CASPT2 level of theory. Otherwise stated, for each geometry, a three roots ($S_0$, $S_1$, $S_2$) state-average (0.33, 0.33, 0.33) CASSCF wavefunction was used as reference function for evaluating the CASPT2 energies.

## 3. Results

### 3.1. Fluorinated chromophores

#### 3.1.1. 2-cis-penta-2,4-dieniminium cation

Minimum energy path (MEP) calculations have been carried out on fluorinated **1** with fluorine substituted at the C1 or C5 positions (the energies of the optimized points along the investigated paths are reported in Table 1). These are the positions where the electronic effect of the substituent is expected to be higher: in fact the positive charge is mainly located nearby the **N**-terminal side (**head**) in the ground state and near the **C**-terminal side (**tail**) in the charge-transfer bright state $S_1$. A schematic view of the $S_0$, $S_1$ and $S_2$ energy profiles along the computed $S_1$ branch of the photoisomerization path of Cl-substituted **1** is shown in Fig. 2 and appears similar to the one previously found for the unsubstituted parent compound **1** [18]: (i) the ground state optimized structure (Min $S_0$) displays the same geometrical characteristic; (ii) at the planar FC point and all along the path, $S_1$ and $S_2$ are well spaced and have an ionic and covalent nature, respectively; (iii) initial relaxation out of the FC region involves only a skeletal (i.e. C–C bonds stretching) rearrangement leading to single/double bond order inversion at the planar stationary point $SP_{standard}$ on $S_1$ (see the $SP_{standard}$ $S_1$ structure in Fig. 2); (iv) from this point (which appears to be a transition state), an orthogonal torsional mode involving OBF twisting of the central double bond is populated, which breaks the planar symmetry of the system; (v) the path is essentially barrierless and leads the system to a peaked $S_1/S_0$ conical intersection (CI $S_1/S_0$) where the central double bond is fully twisted. This point has the form of a TICT-state [12,16,17,20].

The photoisomerization reaction path computed for substitution at C5 appears to be identical to the one described above for C1 substitution and will not be discussed here (the energy values

Table 1
CASPT2/6-31g* absolute (*E*) and relative (Δ*E*) state average path points energies of fluorine-substituted 2-*cis*-penta-2,4-dieniminium cation

| | $S_0$ | | $S_1$ | | $S_2$ | |
|---|---|---|---|---|---|---|
| | *E* (au) | Δ*E* (kcal/mol) | *E* (au) | Δ*E* (kcal/mol) | *E* (au) | Δ*E* (kcal/mol) |
| **$C_1$-F** | | | | | | |
| Min $S_0$ | −347.991267 | 0.0 | −347.839728 | 95.1 | −347.788672 | 127.1 |
| $SP_{standard}$ $S_1$ | −347.972868 | 11.5 | −347.855050 | 85.5 | −347.809639 | 114.0 |
| CI | −347.896187 | 59.7 | −347.890520 | 63.2 | −347.772266 | 137.4 |
| **$C_5$-F** | | | | | | |
| Min $S_0$ | *−347.989796* | *0.0* | *−347.851625* | *86.7* | *−347.790892* | *124.8* |
| $SP_{standard}$ $S_1$ | *−347.974740* | *9.4* | *−347.866728* | *77.2* | *−347.813122* | *110.9* |
| CI | *−347.915114* | *46.9* | *−347.901930* | *55.1* | *−347.773840* | *135.5* |
| | *−346.999422*[a] | *59.4*[a] | *−346.996097*[a] | *61.5*[a] | | |

A three-root CASSCF have been used with equal weights for the states. Active space (8,7). Italicized energy values correspond to points of reaction paths not explicitly discussed and displayed in the figures.

[a] CASSCF two roots state average energy values. AE (kcal/mol) values are calculated by the Min $S_0$ CASSCF two roots state average energies ($S_0$ = −347.094092, $S_1$ = −346.922706).

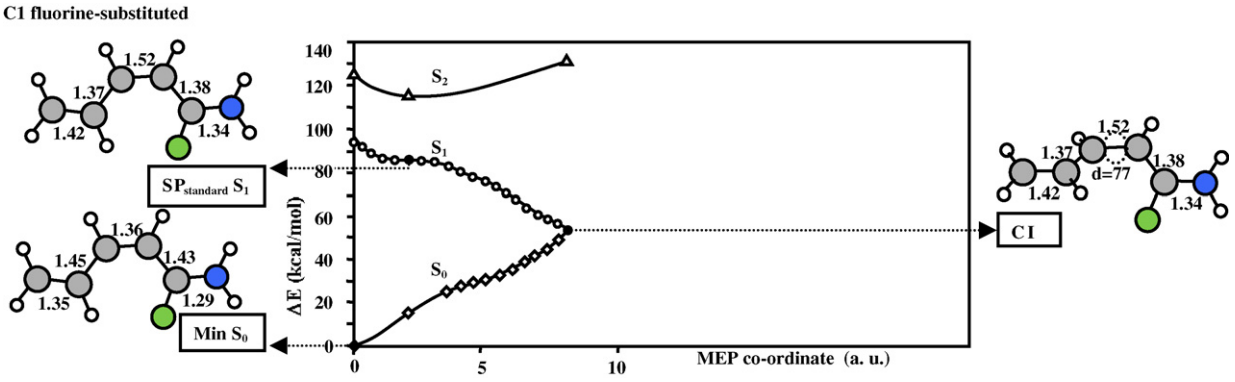


Fig. 2. Computed MEP [16,19] for the isomerization of model **1** substituted with fluorine in position C1. The path has been scaled to match PT2 energy values. The structures (geometrical parameters in Å and degrees) document the geometrical progression along the reaction coordinate. **Min $S_0$** is the minimum structure on $S_0$, **$SP_{standard}$ $S_1$** corresponds to the $S_1$ relaxed planar species, and **CI** is the twisted $S_1/S_0$ conical intersection decay funnel involving the torsion around the central double bond.

for C5 fluorine-substituted **1** are reported in italics in Table 1). Thus, in both cases, the reaction paths keep the same profile of the unsubstituted system and only the spectroscopic properties (i.e. absorption and emission) are modified with respect to the parent compound, as previously shown [31].

### *3.1.2. All-trans-epta-2,4,6-trieniminium cation*

A systematic analysis has been performed for **2** substituted with fluorine in all position along the chain. Vertical excitation energies are reported in Table 2, while the energies of all the optimized points along the investigated paths are reported in Table 3. A qualitatively similar excited state stationary point as found in the parent compound **2** (see $SP_{standard}$ $S_1$ in Fig. 1) was located for the C1, C2, C3, C5 and C7-substituted models, the only differences involving the optical properties [31]. Thus, similar relaxation channels as found in the parent compound **2** are expected departing from this point on $S_1$, i.e. the OBF twisting channels of the two internal double bonds. Anyway, we calculated the minimum energy paths of C2 and C3 fluorinated **2**, i.e. the two systems with a very low and very high photoexcitation energy, respectively (see CASPT2 energy values in Table 2).

Computed MEPs for fluorinated **2** at C2 are reported in Fig. 3a while the energies of the optimized points are reported in Table 3: similarly to unsubtituted **2** [19], the reaction coordinate

Table 2
CASPT2/6-31g* absolute (E) and relative ($\Delta E$) single state vertical excitation energies for fluorine-substituted 2-*cis*-penta-2,4-dieniminium cation (**1**) and fluorine and methoxy-substituted all-*trans*-epta-2,4,6-trieniminium cation **(2)**

| | $S_0$ (au) | $S_1$ (au) | $\Delta E$ $S_0 \rightarrow S_1$ (kcal/mol) | $\lambda$ $S_0 \rightarrow S_1$ (nm) |
|---|---|---|---|---|
| **1 Min $S_0$**[a] | −248.969935 | −248.82374 | 91.7 | 312 |
| **$C_1$-F Min $S_0$**[b] | −347.98724 | −347.83456 | 95.8 | 298 |
| **$C_2$-F Min $S_0$**[b] | −347.97504 | −347.83788 | 86.1 | 332 |
| **$C_3$-F Min $S_0$**[b] | −347.98825 | 347.83552 | 95.8 | 298 |
| **$C_4$-F Min $S_0$**[b] | −347.98762 | −347.84284 | 90.8 | 315 |
| **$C_5$-F Min $S_0$**[b] | −347.98405 | −347.84795 | 85.4 | 335 |
| **2 Min $S_0$**[c] | −326.12346[b] | −326.006327[b] | 73.5 | 389 |
| **C1-F Min $S_0$**[d] | −425.14111 | −425.02038 | 75.8 | 377 |
| **C2-F Min $S_0$**[d] | −425.13375 | −425.02301 | 69.5 | 411 |
| **C3-F Min $S_0$**[d] | −425.14279 | −425.02148 | 76.1 | 376 |
| **C4-F Min $S_0$**[d] | −425.13756 | −425.02695 | 69.4 | 412 |
| **C5-F Min $S_0$**[d] | −425.14332 | −425.02586 | 73.7 | 388 |
| **C6-F Min $S_0$**[d] | −425.13925 | −425.02353 | 72.6 | 394 |
| **C7-F Min $S_0$**[d] | −425.13999 | −425.02714 | 70.8 | 408 |
| **C1-OCH3 Min $S_0$**[e] | −440.32840 | −440.19665 | 82.7 | 346 |
| **C2-OCH3 Min$S_0$**[e] | −440.31002 | −440.19450 | 72.5 | 394 |
| **C3-OCH3 Min $S_0$**[e] | −440.31756 | −440.18984 | 80.1 | 357 |
| **C4-OCH3 Min $S_0$**[e] | −440.30825 | −440.19833 | 69.0 | 414 |
| **C5-OCH3 Min $S_0$**[e] | −440.31332 | −440.20179 | 70.0 | 408 |
| **C6-OCH3 Min $S_0$**[e] | −440.31536 | −440.21115 | 65.4 | 437 |
| **C7-OCH3 Min $S_0$**[e] | −440.31996 | −440.29963 | 56.7 | 504 |

[a] Active space (6,6).
[b] Active space (8,7).
[c] Active space (8,8).
[d] Active space (10,9).
[e] Active space (12,10).

Table 3
CASPT2/6-31g* absolute ($E$) and relative ($\Delta E$) state average path points energies of fluorine-substituted all-*trans*-epta-2,4,6-trieniminium cation

| | $S_0$ | | $S_1$ | | $S_2$ | |
|---|---|---|---|---|---|---|
| | $E$ (au) | $\Delta E$ (kcal/mol) | $E$ (au) | $\Delta E$ (kcal/mol) | $E$ (au) | $\Delta E$ (kcal/mol) |
| **$C_1$-F** | | | | | | |
| Min $S_0$ | *−425.150902* | *0.0* | *−425.027251* | *77.6* | *−424.984143* | *104.6* |
| $SP_{standard}$ $S_1$ | *−425.135592* | *9.6* | *−425.036033* | *72.1* | *−425.001063* | *94.0* |
| **$C_2$-F** | | | | | | |
| Min $S_0$ | −425.144459 | 0.0 | −425.032838 | 70.0 | −424.994005 | 94.4 |
| $SP_{standard}$ $S_1$ | −425.128845 | 9.8 | −425.043704 | 63.2 | −425.006307 | 86.7 |
| CI $d_1$ | −425.066372 | 49.0 | −425.064244 | 50.3 | −424.974608 | 106.6 |
| CI $d_2$ | −425.065722 | 49.4 | −425.060506 | 52.7 | −424.968504 | 110.4 |
| **$C_3$-F** | | | | | | |
| Min $S_0$ | −425.152899 | 0.0 | −425.032009 | 75.9 | −424.990946 | 101.6 |
| $SP_{standard}$ $S_1$ | −425.135809 | 10.7 | −425.045160 | 67.6 | −425.003422 | 93.8 |
| TM $d_1$ | −425.087890 | 40.8 | −425.057585 | 59.8 | −424.962520 | 119.5 |
| CI $d_2$ | *−425.067903* | *53.3* | *−425.065456* | *54.9* | *−424.981098* | *107.8* |
| **$C_4$-F** | | | | | | |
| Min $S_0$ | −425.147810 | 0.0 | −425.033333 | 71.8 | −424.988827 | 100.0 |
| $SP_{anomalous}$ $S_1$ | −425.145210 | 1.6 | −425.040977 | 67.0 | −425.006677 | 88.6 |
| TS $d_1$ | −425.143842 | 2.5 | −425.040836 | 67.1 | −425.004311 | 90.0 |
| CI $d_1$ | −425.076060 | 45.0 | −425.068688 | 49.6 | −424.971533 | 110.6 |
| CI $d_2$ | *−423.90446*[a] | *73.1*[a] | *−423.90537*[a] | *72.5*[a] | | |
| **$C_5$-F** | | | | | | |
| Min $S_0$ | *−425.154022* | *0.0* | *−425.032554* | *76.2* | *−424.988957* | *103.6* |
| $SP_{standard}$ $S_1$ | *−425.135308* | *11.7* | *−425.042747* | *69.8* | *−425.001993* | *95.4* |
| **$C_6$-F** | | | | | | |
| Min $S_0$ | −425.149627 | 0.0 | −425.029477 | 75.4 | −424.989108 | 100.7 |
| $SP_{anomalous}$ $S_1$ | −425.145444 | 2.6 | −425.037304 | 70.5 | −425.007426 | 89.2 |
| RI $d_1$ | −425.141492 | 5.1 | −425.039504 | 69.1 | −425.012088 | 86.3 |
| CI $d_1$ | −425.075248 | 46.7 | −425.068629 | 50.8 | −424.977075 | 108.3 |
| TM $d_2$ | −425.071296 | 49.1 | −425.051181 | 61.8 | −424.973635 | 110.4 |
| **$C_7$-F** | | | | | | |
| Min $S_0$ | *−425.151030* | *0.0* | *−425.032872* | *74.1* | *−424.988158* | *102.2* |
| $SP_{standard}$ $S_1$ | *−425.134053* | *10.7* | *−425.040569* | *69.3* | *−425.004916* | *91.7* |

A three-root CASSCF have been used with equal weights for the states. Active space (8,8). Italicized energy values correspond to points of reaction paths not explicitly discussed and displayed in the figures.

[a] CASSCF 6-31g* values, using a two roots ($S_1$ and $S_0$) state average procedure. AE (kcal/mol) value is calculated by the Min $S_0$ CASSCF two roots state average energies ($S_0 = -424.02095$, $S_1 = -423.87449$).

is bimodal with two competing and barrierless isomerization paths departing from the $SP_{standard}$ stationary point on $S_1$ (see the $SP_{standard}$ $S_1$ structure in Fig. 3a), which is located at the centre of an extended energy plateau (note that the extension of this plateau increases as increasing the chain length of the chosen PSB model, i.e. **1** or **2**). Each path involves the OBF twisting of one of the two central double bonds (i.e. rotation of C1−C2=C3−C4 ($d_1$) and C3−C4=C5−C6 ($d_2$) dihedral angles, respectively) and leads to a twisted $S_1/S_0$ CI, very similarly to what seen above for C1-fluorinated **1**.

Although qualitatively similar, the C3-substituted model shows same differences in comparison with **2**. Fig. 3b shows the isomerization path about the dihedral angle $d_1$ computed for this system. It is apparent that the reaction path does not end into a $S_1/S_0$ crossing region, which is replaced by a twisted minimum (TM $d_1$, see Fig. 3b and Table 3). This behavior suggests that non-radiative decay and photoisomerization for this system could be slower (i.e. longer excited state life time) and less efficient (i.e. smaller quantum yield) as compared to **2**. Anyway, all the remaining of the reaction path is qualitatively comparable to that of the parent system. As stated above, this is absolutely unsurprising looking at the $SP_{standard}$ structure. Furthemore, isomerization about $d_2$ for C3 fluorine-substituted is identical to that of the parent compound **2**, and is not reported here (the corresponding energy values are reported in Table 3 in italics).

On the other hand, C4 and C6 fluorinated systems show the most serious and significant differences in photochemical reactivity. Initial relaxation out of the FC point (involving a C–C bonds rearrangement) leads to a different planar stationary point ($SP_{anomalous}$) that displays very less stretched/compressed single/double bonds as compared to the one found in the parent compound ($SP_{standard}$), see the $SP_{anomalous}$ $S_1$ structures in Fig. 3c–e (see Table 3 for the energy values). Note that both the standard ($SP_{standard}$) and anomalous ($SP_{anomalous}$) stationary points exist at the CASSCF level on the $S_1$ surface (see Table 4); anyway, CASPT2 corrected profiles exhibit only the anomalous one since its structure is stabilized while that of $SP_{standard}$ is destabilized (Fig. 4). Anyway, after this starting anomalous

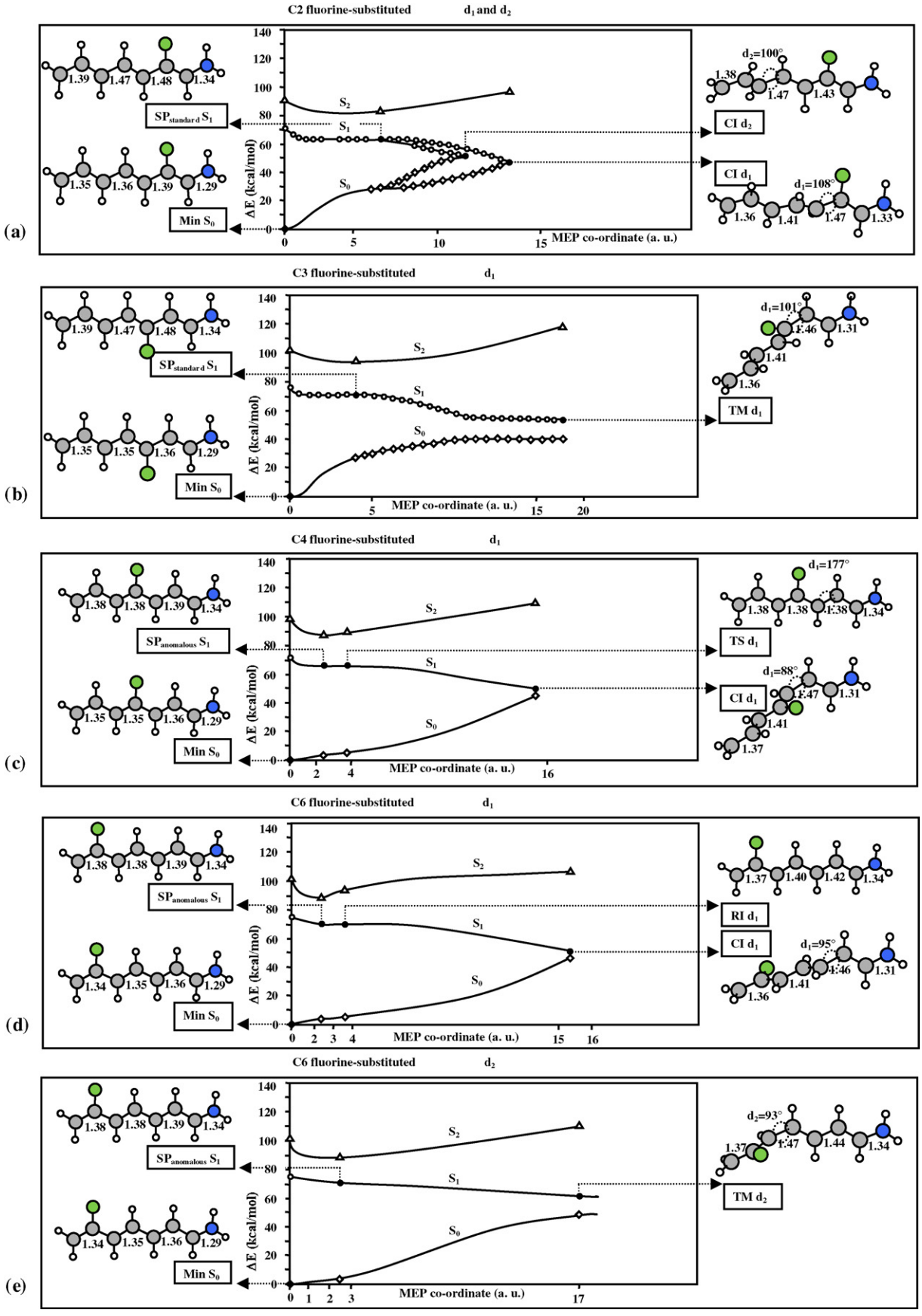
(a)
C2 fluorine-substituted d1 and d2
SP standard S1
Min S0
CI d2
CI d1
d2=100°
d1=108°
ΔE (kcal/mol)
MEP co-ordinate (a. u.)
(b)
C3 fluorine-substituted d1
SP standard S1
Min S0
TM d1
d1=101°
ΔE (kcal/mol)
MEP co-ordinate (a. u.)
(c)
C4 fluorine-substituted d1
SP anomalous S1
Min S0
TS d1
CI d1
d1=177°
d1=88°
ΔE (kcal/mol)
MEP co-ordinate (a. u.)
(d)
C6 fluorine-substituted d1
SP anomalous S1
Min S0
RI d1
CI d1
d1=95°
ΔE (kcal/mol)
MEP co-ordinate (a. u.)
(e)
C6 fluorine-substituted d2
SP anomalous S1
Min S0
TM d2
d2=93°
ΔE (kcal/mol)
MEP co-ordinate (a. u.)

Table 4
CASPT2/6-31g* absolute ($E$) and relative ($\Delta E$) single state energies for the stationary point $S_1$ structure ($SP_{standard}$ or $SP_{anomalous}$) of fluorine-substituted 2-*cis*-penta-2,4-dieniminium cation (1) and fluorine and methoxy-substituted all-*trans*-epta-2,4,6-trieniminium cation (**2**)

| | $S_0$ (au) | $S_1$ (au) | $\Delta E$ $S_0 \rightarrow S_1$ (kcal/mol) | $\lambda$ $S_0 \rightarrow S_1$ (nm) |
|---|---|---|---|---|
| **1** $SP_{anomalous}$ [a] | −248.96370 | −248.83425 | 81.2 | 352 |
| **1** $SP_{standard}$ [a] | −248.94855 | −248.82911 | 74.9 | 382 |
| **$C_1$-F** $SP_{standard}$ [b] | −347.96789 | −347.84552 | 76.8 | 372 |
| **$C_5$-F** $SP_{standard}$ [b] | −347.96806 | −347.85462 | 71.2 | 402 |
| **2** $SP_{standard}$ [c] | −326.10945 | −326.01417 | 59.8 | 478 |
| **C1-F** $SP_{standard}$ [c] | −425.13102 | −425.03413 | 60.8 | 470 |
| **C2-F** $SP_{standard}$ [c] | −425.12266 | −425.03523 | 54.9 | 521 |
| **C3-F** $SP_{standard}$ [c] | −425.13028 | −425.03673 | 58.7 | 487 |
| **C4-F** $SP_{anomalous}$ [c] | −425.13371 | −425.03407 | 62.5 | 457 |
| **C4-F** $SP_{standard}$ [c] | −425.11971 | −425.02777 | 57.7 | 495 |
| **C5-F** $SP_{standard}$ [c] | −425.13057 | −425.04085 | 56.3 | 508 |
| **C6-F** $SP_{anomalous}$ [c] | −425.13446 | −425.03125 | 64.8 | 441 |
| **C6-F** $SP_{standard}$ [c] | −425.11680 | −425.02515 | 57.5 | 497 |
| **C7-F** $SP_{standard}$ [c] | −425.12855 | −425.03821 | 56.7 | 504 |
| **C1-$OCH_3$** $SP_{standard}$ [d] | −440.31281 | −440.21285 | 62.7 | 456 |
| **C2-$OCH_3$** $SP_{standard}$ [d] | −440.29480 | −440.21084 | 52.7 | 442 |
| **C3-$OCH_3$** $SP_{standard}$ [d] | −440.30061 | −440.20835 | 57.9 | 493 |
| **C4-$OCH_3$** $SP_{anomalous}$ [d] | −440.30698 | −440.21165 | 59.8 | 478 |
| **C4-$OCH_3$** $SP_{standard}$ [d] | −440.30585 | −440.20465 | 63.5 | 450 |
| **C5-$OCH_3$** $SP_{standard}$ [d] | −440.31143 | −440.22709 | 52.9 | 540 |
| **C6-$OCH_3$** $SP_{anomalous}$ [d] | −440.31128 | −440.22543 | 53.9 | 530 |
| **C7-$OCH_3$** $SP_{standard}$ [d] | −440.32391 | −440.24196 | 51.4 | 556 |

[a] Active space (6,6).
[b] Active space (8,7).
[c] Active space (8,8).
[d] Active space (10,9).

stretching mode, the standard and usual reaction path is restored by following the same decay channel of the parent compound: double bonds become longer and at the same time the twisting mode about the two central double bonds (i.e. rotation of $d_1$ and $d_2$, respectively) become accessible. In the C4 fluorine-substituted $d_1$ twisting case (Fig. 3c) the system reaches a fully twisted $S_1/S_0$ CI (CI $d_1$) through a very flat path (that involves even a tiny transition state, TS $d_1$). In the $d_2$ case (Table 3, italicized line) the $S_1$ profile shows the same behavior of the $d_1$ isomerization path, although the TS to reach to $S_1/S_0$ conical intersection (CI $d_2$) is absent. Fig. 3d shows the computed $d_1$ twisting path for C6-substituted **2**: it leads to the fully twisted $S_1/S_0$ CI (CI $d_1$) through a very flat path that involves a small transition state only at CASSCF level (RI $d_1$). In the $d_2$ isomerization case (Fig. 3e) the $S_1$ profile does not show any barrier, but is featured by a twisted minimum (not a real crossing) at its end (TM $d_2$).

In conclusion, while C3, C4 or C6-substituted **2** show a reaction mechanism which is in qualitative agreement with the one found for the parent compound (i.e. easily accessible OBF isomerization paths for the central double bonds on $S_1$), the possible existence of a flatter isomerization path (or even of a tiny barrier) and of a twisted minimum instead of a CI, is expected to affect the lifetime, the rate and the efficiency of the isomerization photo-induced process.

### 3.2. Methoxy-substituted chromophores

#### 3.2.1. All-trans-epta-2,4,6-trieniminium cation

An analysis has been performed for **2**, which has been systematically substituted with methoxyl in all the position along the chain. Vertical excitation energies are reported in Table 2, while the energies of all the optimized points along the investigated

Fig. 3. (a) Computed MEPs [16,19] for the isomerization of model **2** substituted with fluorine in position C2. The paths have been scaled to match PT2 energy values. The structures (geometrical parameters in Å and degrees) document the geometrical progression along the reaction coordinate. **Min $S_0$** is the minimum structure on $S_0$, **$SP_{standard}$ $S_1$** corresponds to the $S_1$ relaxed planar species, and **CI $d_1$** and **CI $d_2$** are the competitive twisted $S_1/S_0$ conical intersection decay funnels involving the torsion around the C2═C3 ($d_1$) and C4═C5 ($d_2$) double bonds, respectively. (b) Computed MEP for the $d_1$ isomerization of model **2** substituted with fluorine in position C3. **$SP_{standard}$ $S_1$** corresponds to the $S_1$ relaxed planar species **and TM $d_1$** is the twisted $S_1$ minimum involving the torsion around the C2═C3 ($d_1$) double bond. (c) Computed MEP for the $d_1$ isomerization of model **2** substituted with fluorine in position C4. **$SP_{anomalous}$ $S_1$** corresponds to the $S_1$ anomalous relaxed planar specie that displays very less stretched/compressed single/double bonds as compared to the one found in the parent compound ($SP_{standard}$). **TS $d_1$** is the transition state structure and **CI $d_1$** is the twisted $S_1/S_0$ conical intersection decay funnels involving the torsion around the C2═C3 ($d_1$) double bond. (d) Computed MEP for the $d_1$ isomerization of model **2** substituted with fluorine in position C6. **$SP_{anomalous}$ $S_1$** corresponds to the $S_1$ anomalous relaxed planar specie, **RI $d_1$** is the reaction intermediate structure coinciding with the transition state at the CASSCF level, and **CI $d_1$** is the twisted $S_1/S_0$ conical intersection decay funnel involving the torsion around the C2═C3 ($d_1$) double bond. (e) Computed MEP for the $d_2$ isomerization of model **2** substituted with fluorine in position C6. **$SP_{anomalous}$ $S_1$** corresponds to the $S_1$ anomalous relaxed planar specie and **TM $d_2$** is the twisted $S_1$ minimum involving the torsion around the C4═C5 ($d_2$) double bond.

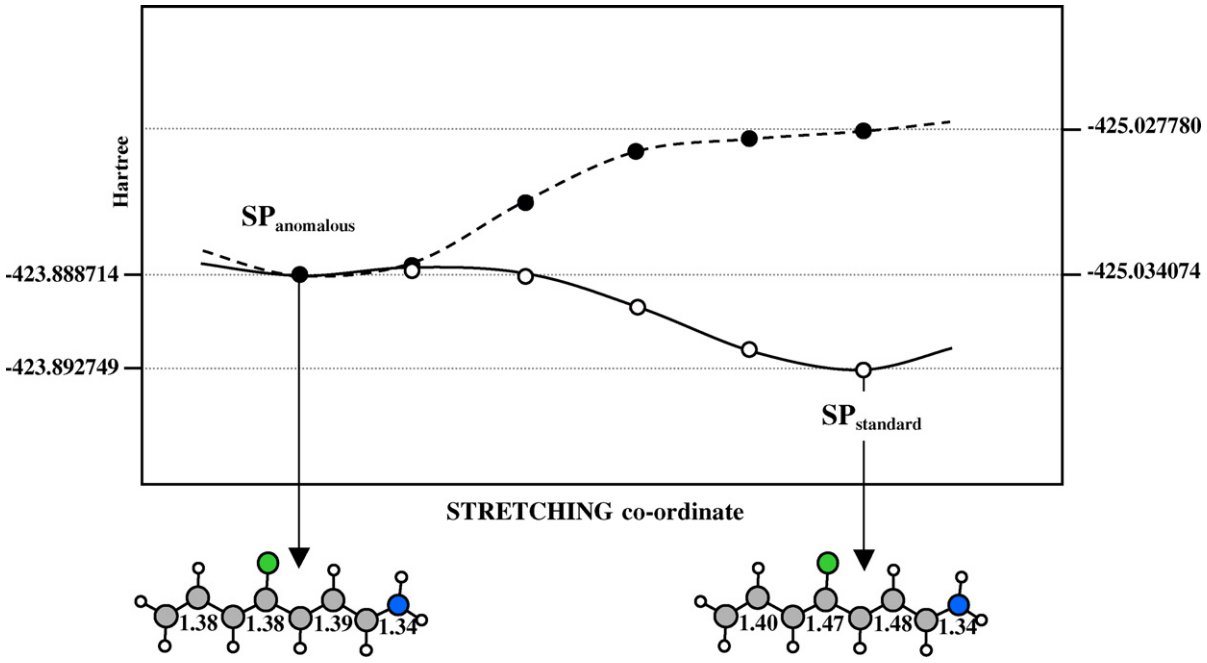


Fig. 4. CASSCF energy profile (full line: reference energies (hartree) are reported on the left vertical axe) and CASPT2 S1 energy profile (dotted line: reference energies (hartree) are reported on the right vertical axe) connecting the standard and anomalous SP point of C4-fluorinated **2**. Additional points (by a linear interpolation) have been added. Single state computations have been used with an active space of 8 electrons in 8 orbitals and the 6-31g* basis set. Bond lengths are reported in Å.

paths are reported in Table 5. The planar relaxation out of the FC region computed along the $S_1$ MEPs has been compared for each substituted system with that found in the parent compound **2**. It results that only C4, C6 and C7 methoxy-substituted systems show a different stationary point compared to the $SP_{standard}$ of **2**. All the other substitutions, which lead to the same $SP_{standard}$ point as found in **2**, are not further analyzed and discussed since their photo-reactivity is similar and comparable to that of the parent compound.

C4 methoxy-substituted **2** has a very peculiar behavior. Following the initial relaxation out of FC, that leads the system to the planar $SP_{anomalous}$ relaxed structure ($SP_{anomalous}$ $S_1$ in Fig. 5a), a new reaction path was found while the usual isomerization channels about $d_1$ and $d_2$ are prevented: this involves a barrierless isomerization about the C3–C4 single bond, which leads to a deep twisted minimum at $\phi = 92^\circ$ (TM $d_3$). This point is connected to a sloped $S_1/S_0$ CI (CI $d_3$), which is anyway too far higher in energy to be photochemically relevant. Thus, once the anomalous stationary point ($SP_{anomalous}$ $S_1$) is populated, the system starts the isomerization around the central C3–C4 single bond ($d_3$ dihedral angle) whose rotation is very easy since this bond is very much stretched at the $SP_{anomalous}$ structure. This is the only substituted compound, among all the systems considered here, whose photochemical behavior changes qualitatively upon substitution (i.e. a different photoisomerization path exists). Furthermore, we have computationally verified that there is no chance to populate the path that leads to isomerization around the C5–C6 single bond ($d_4$) or to OBF twisting about one of the two internal double bonds ($d_1$ and $d_2$ dihedral angles) as found in the parent compound.

The C6 methoxy-substituted **2** follows an initial relaxation on $S_1$ that leads to the previously described anomalous stationary point ($SP_{anomalous}$ $S_1$, Fig. 5b). From there, two competing OBF photoisomerization paths exist that are characterized by a low-energy transition state (TS $d_1$ and TS $d_2$ in Fig. 5b and c, respectively) along a reaction coordinate given by a combination of both stretching and twisting modes, which restores the isomerization channel found in the parent compound. These channels drive the systems to a twisted structure that is a minimum (TM $d_1$, see Fig. 5b) or a conical intersection (CI $d_2$, see Fig. 5c) for isomerization about $d_1$ or $d_2$, respectively. A sloped $S_1/S_0$ CI (CI $d_1$) has been also located, which is connected to TM $d_1$ and higher in energy. Anyway, qualitatively, nothing changes in the reactivity with respect to the parent compound, although longer excited state life times and less efficient photoisomerizations (i.e. smaller quantum yields) are expected. Note that at the CASSCF level, a fully twisted minimum exists on $S_1$ about both the $d_3$ and $d_4$ isomerization paths, which is higher in energy than $SP_{anomalous}$ and that can be populated thought a small transition state (see Table 5). Anyway, at the CASPT2 level the topography of the $S_1$ surface changes and the twisted minima turn out to be transition states, preventing these paths as efficient internal conversion routes (Table 5).

The C7 methoxy-substituted **2** follows an initial relaxation on $S_1$ that leads to the standard stationary point ($SP_{standard}$ $S_1$, Fig. 5d), although its double bonds are a little bit shorter than for $SP_{standard}$ found in **2** (Fig. 1). Fig. 4d illustrates the computed reaction path for rotation about $d_1$: it is apparent that the path is very flat, spanning an extended energy plateau on the $S_1$ PES and involving simultaneously a stretching (that leads to a full C–C bonds order inversion) and a $d_1$ twisting mode (note that RI $d_1$

Table 5
CASPT2/6-31g* absolute ($E$) and relative ($\Delta E$) state average path points energies of methoxy-substituted all-*trans*-epta-2,4,6-trieniminium cation

| | $S_0$ | | $S_1$ | | $S_2$ | |
|---|---|---|---|---|---|---|
| | $E$ (au) | $\Delta E$ (kcal/mol) | $E$ (au) | $\Delta E$ (kcal/mol) | $E$ (au) | $\Delta E$ (kcal/mol) |
| **$C_1$-$OCU_3$** | | | | | | |
| Min $S_0$ | *−440.338250* | *0.0* | *−440.203800* | *84.4* | *−440.164374* | *109.1* |
| $SP_{standard}$ $S_1$ | *−440.317357* | *13.1* | *−440.214026* | *77.9* | *−440.187644* | *94.5* |
| **$C_2$-$OCH_3$** | | | | | | |
| Min $S_0$ | *−440.320379* | *0.0* | *−440.202257* | *74.1* | *−440.168414* | *95.4* |
| $SP_{standard}$ $S_1$ | *−440.299558* | *13.1* | *−440.212909* | *67.4* | *−440.179520* | *88.4* |
| **$C_3$-$OCH_3$** | | | | | | |
| Min $S_0$ | *−440.324289* | *0.0* | *−440.192651* | *82.6* | *−440.174711* | *93.9* |
| $SP_{standard}$ $S_1$ | *−440.305378* | *11.9* | *−440.210811* | *71.2* | *−440.176375* | *92.8* |
| **$C_4$-$OCH_3$** | | | | | | |
| Min $S_0$ | −440.320059 | 0.0 | −440.206653 | 71.1 | −440.164221 | 97.8 |
| $SP_{anomalous}$ $S_1$ | −440.314796 | 3.3 | −440.215132 | 65.8 | −440.177143 | 89.7 |
| TM $d_3$ | −440.265471 | 34.2 | −440.247688 | 45.4 | −440.149789 | 106.8 |
| CI $d_3$ | −440.211733 | 68.0 | −440.200162 | 75.2 | −440.115686 | 128.2 |
| | −438.926052[a] | 79.8[a] | −438.924245[a] | 80.9[a] | | |
| **$C_5$-$OCH_3$** | | | | | | |
| Min $S_0$ | *−440.323956* | *0.0* | *−440.208954* | *72.1* | *−440.162508* | *101.3* |
| $SP_{standard}$ $S_1$ | *−440.314051* | *6.2* | *−440.229818* | *59.1* | *−440. 171535* | *95.6* |
| **$C_6$-$OCH_3$** | | | | | | |
| Min $S_0$ | −440.327636 | 0.0 | −440.220132 | 67.5 | −440.183994 | 90.1 |
| $SP_{anomalous}$ $S_1$ | −440.319440 | 5.1 | −440.229346 | 61.7 | −440.192434 | 84.8 |
| TS $d_1$ | −440.308184 | 12.2 | −440.217258 | 69.3 | −440.198581 | 81.0 |
| TM $d_1$ | −440.255712 | 45.1 | −440.240076 | 54.9 | −440.152756 | 109.7 |
| CI $d_1$ | −440.210626 | 73.4 | −440.198861 | 80.8 | −440.112893 | 134.7 |
| | −440.209005[a] | 72.8[b] | −440.203372[b] | 76.3[b] | | |
| TS $d_2$ | −440.297875 | 18.7 | −440.219893 | 67.6 | −440.188713 | 87.1 |
| CI $d_2$ | −440.257853 | 43.8 | −440.241858 | 53.8 | −440.155164 | 108.2 |
| | −440.236726[b] | 55.4[b] | −440.230536[b] | 59.3[b] | | |
| TS $d_3$ | *−440.287248* | *24.3* | *−440.222170* | *66.2* | *−440.153114* | *109.5* |
| TM $d_3$ | *−440.275997* | *32.4* | *−440.220788* | *67.0* | *−440.150795* | *111.0* |
| TS $d_4$ | *−440.286286* | *25.9* | *−440.222554* | *65.9* | *−440.158178* | *106.3* |
| TM $d_4$ | *−440.278144* | *31.0* | *−440.221897* | *66.3* | *−440.147620* | *113.0* |
| **$C_7$-$OCH_3$** | | | | | | |
| Min $S_0$ | −440.333072 | 0.0 | −440.235629 | 61.1 | −440.185900 | 92.3 |
| $SP_{standard}$ $S_1$ | −440.331236 | 1.1 | −440.243395 | 56.3 | −440.203249 | 81.5 |
| RI $d_1$ | −440.307120 | 16.3 | −440.244245 | 55.7 | −440.184566 | 93.2 |
| TM $d_1$ | −440.245555 | 54.9 | −440.275432 | 36.2 | −440.149598 | 115.2 |
| CI $d_1$ | −440.235012 | 61.5 | −440.222877 | 69.1 | −440.130169 | 127.3 |
| | −440.229888[c] | 63.6[c] | −440.225980[c] | 66.0[c] | | |
| RI $d_2$ | *−440.309775* | *14.6* | *−440.244425* | *55.6* | *−440.183373* | *93.9* |
| TM $d_2$ | *−440.256506* | *48.0* | *−440.267283* | *41.3* | *−440.153571* | *112.6* |
| CI $d_2$ | *−440.234750* | *61.7* | *−440.230530* | *64.3* | *−440.134490* | *124.6* |

A three-root CASSCF have been used with equal weights for the states. Active space (10,9). Italicized energy values correspond to points of reaction paths not explicitly discussed and displayed in the figures.

[a] CASSCF two roots state average energy values. $\Delta E$ (kcal/mol) value is calculated by the Min $S_0$ CASSCF two roots state average energies ($S_0 = -439.053187$, $S_1 = -438.908756$).

[b] CASPT2 two roots state average energy values. $\Delta E$ (kcal/mol) value is calculated by the Min $S_0$ CASPT2 two roots state average energies ($S_0 = -440.325053$, $S_1 = -440.219263$).

[c] CASPT2 two roots state average energy values. $\Delta E$ (kcal/mol) value is calculated by the Min $S_0$ CASPT2 two roots state average energies ($S_0 = -440.331231$, $S_1 = -440.235082$).

is a transition state at the CASSCF level, which disappears after PT2 corrections). This very flat barrierless path eventually leads to a twisted minimum (TM $d_1$), which is only slightly lower in energy than SP and is connected to a higher energy sloped $S_1/S_0$ CI (CI $d_1$). The other competitive isomerization path about $d_2$ is identical (see Table 5, italicized line) and will not be displayed here. Note that the isomerization mechanism is qualitatively the same as for **2**.

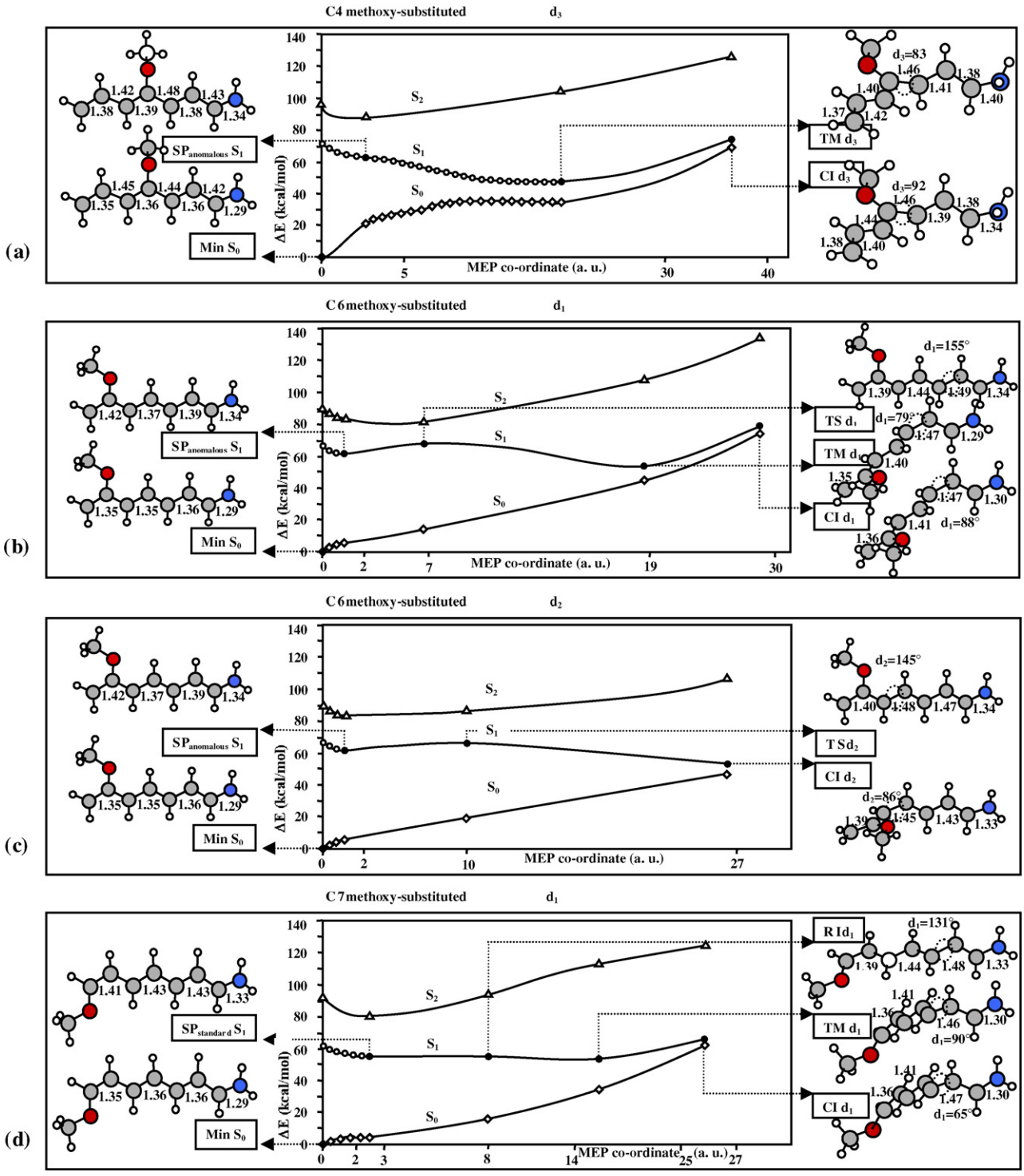


Fig. 5. (a) Computed MEP [16,19] for the $d_3$ isomerization of model **2** substituted with methoxyl in position C4. The path has been scaled to match PT2 energy values. The structures (geometrical parameters in Å and degrees) document the geometrical progression along the reaction coordinate. **Min $S_0$** is the minimum structure on $S_0$, **$SP_{anomalous}$ $S_1$** corresponds to the $S_1$ anomalous relaxed planar specie that displays very less stretched/compressed single/double bonds as compared to the one found in the parent compound ($SP_{standard}$). TM **$d_3$** is the twisted $S_1$ minimum involving the torsion around the C3═C4 ($d_3$) single bond and **CI $d_3$** is the sloped twisted $S_1/S_0$ conical intersection decay funnels involving the torsion around the dihedral angle $d_3$. (b) Computed MEP for the $d_1$ isomerization of model **2** substituted with methoxyl in position C6. **$SP_{anomalous}$ $S_1$** corresponds to the $S_1$ anomalous relaxed planar specie, **TS $d_1$** is the transition state structure, **TM $d_1$** is the twisted $S_1$ minimum involving the torsion around the C2═C3 ($d_1$) double bond and **CI $d_1$** is the sloped twisted $S_1/S_0$ conical intersection decay funnels involving the torsion around the dihedral angle $d_1$. (c) Computed MEP for the $d_2$ isomerization of model **2** substituted with methoxyl in position C6. **$SP_{anomalous}$ $S_1$** is to the $S_1$ anomalous relaxed planar specie (the same of Fig. 5b), **TS $d_2$** is the transition state structure and **CI $d_2$** is the twisted peaked $S_1/S_0$ conical intersection decay funnels involving the torsion around the C4═C5 ($d_2$) double bond. (d) Computed MEP for the $d_1$ isomerization of model **2** substituted with methoxyl in position C7. **$SP_{anomalous}$ $S_1$** corresponds to the $S_1$ anomalous relaxed planar specie, **RI $d_1$** is the reaction intermediate structure coinciding with the transition state at the CASSCF level, **TM $d_1$** is the twisted $S_1$ minimum involving the torsion around the C2═C3 ($d_1$) double bond and **CI $d_1$** is the twisted $S_1/S_0$ conical intersection decay funnels involving $d_1$ dihedral angle torsion.

## 4. Discussion

### 4.1. Substituent effect on the SP point: analysis and interpretation

The computational results presented in the section above shown how fluorine and methoxyl substituents (which possess an opposite electronic effect: electron-withdrawing and electron-releasing, respectively) may influence and modify the photochemical reactivity of retinal chromophore models. In summary, it has been shown that most of the substituted systems does substantially preserve the photochemical properties of the unsubstituted parent compounds: barrierless isomerization paths exist on the spectroscopic charge transfer $S_1$ state, which involve a OBF rotation of each one of the central double bonds. $S_2$ (as $S_0$) preserves a covalent nature with the positive charge centered on the **head** (i.e. the **N**-terminal side) and remains energetically higher than $S_1$ along the whole reaction profile. Initially, a planar stationary point ($SP_{standard}$) is populated with an inverted single/double bond pattern, which therefore triggers an energetically costless OBF isomerization of the central double bonds leading eventually to the fully twisted deactivation funnel (i.e. the $S_1/S_0$ CI or $S_1$ minimum). Only C4 and C6 fluorine and methoxy-substituted systems do show different (quantitative and/or qualitative) photochemical behaviors (see section above). At a first sight, this appears quite surprising since one could expect that reaction paths are mostly modified in the case of **head** or **tail**-substituted positions: it is here where the majority of the charge resides in the ground and ionic $S_1$ state, respectively, and it is here, in fact, where the electronic effects of the substituents are expected to be higher.

A rationale for this behavior may be provided if we look at the structure of the relaxed stationary point SP on $S_1$, which is initially populated by decay from the FC region. We have seen that, while for most of the systems (including the parent compounds **1** and **2**) the typical single/double bond inverted pattern is observed for the geometry of the stationary point on $S_1$ ($SP_{standard}$), for C4 and C6-substituted systems a structurally anomalous stationary point is populated ($SP_{anomalous}$) with very less stretched C=C double bonds and less compressed C–C single bonds. Thus, it is evident that different (quantitative and/or qualitative) isomerization paths arise from a different stationary point (i.e. a different initial planar relaxation out of the FC region) where, in fact, these isomerization processes do start. Furthermore, it is worth to note that, for many systems (i.e. C4 and C6 fluorinated **2**, C4 methoxy-substituted **2** and the parent compound **1** as well, see the discussion above), both structures $SP_{standard}$ and $SP_{anomalous}$ exist on $S_1$ at the CAS-SCF level, which are almost degenerate and are separated by a transition state (see Fig. 4 for an example). Anyway, when CAS-PT2 corrections are applied, only one of the two SP structures survives with the other one being destabilized (as shown by the CAS-PT2 corrected path in Fig. 4). In particular, C4 and C6 fluorinated and methoxy-substituted **2** exhibit only the anomalous SP structure at the CAS-PT2 level.

The existence in several systems (e.g. the parent compound **1**) of both almost-degenerate SP points (at the CAS-SCF level) suggests the possibility for a substituent to tune their relative stability depending on its electronic effects. Computational results show that this suggestion is indeed found and that the substituent, when it is placed in a specific position (namely C4 and C6), do affect the shape of the excited state leading to the emergence of a stable anomalous SP point, i.e. they do stabilize this structure. Thus, it appears that the energy lowering effect on the anomalous SP point due to substitution is major only for positions C4 and C6 (whatever it is the specific electronic effect of the substituent). An understanding for that may be achieved if we look at the different Mulliken charge distribution in the $SP_{anomalous}$ and $SP_{standard}$ states. Such an analysis shows an increasing positive charge density for the anomalous SP point at C4 and C6 as compared to the standard SP structure (see Scheme 3). Therefore, since both substituents do stabilize neighboring positive charges (by electron-releasing mesomeric effect and through the methoxy oxygen and fluorine atom it electron cloud that spans over adjacent carbon atoms, see Scheme 3), C4 and C6 substitutions stabilize the anomalous SP structure more than the standard one and the anomalous point becomes more stable. A more general characterization in terms of electronic structure of both the anomalous and standard SP minima has been achieved via $P_{ij}$'s (*spin exchange density matrix elements*) and $D_{ii}$'s (*diagonal elements of the first-order density matrix*) analysis. This delivers a detailed description of bond orders, electronic occupations and charge translocation. The interested reader is referred to Appendix A for the results of this deeper investigation.

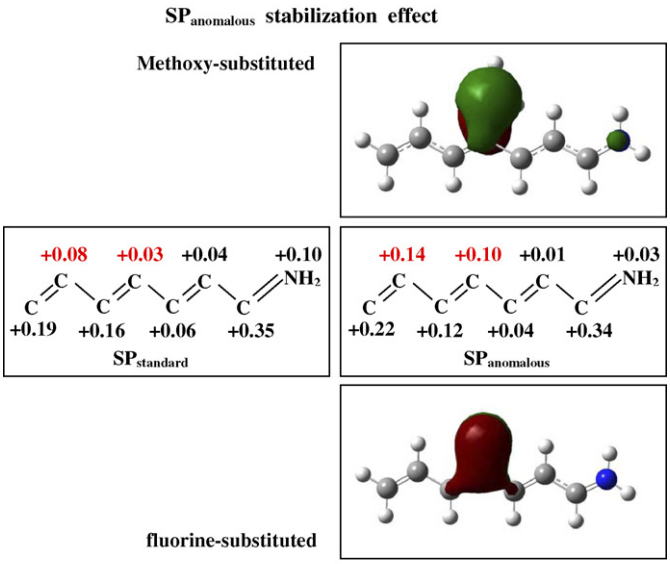


Scheme 3.

### 4.2. Substituent effect on the photochemical reaction paths: a unified reactivity scheme

It is worth noting that the existence of one or the other of the two SP structures is not a purely academic issue: as it has been shown above, SP (which is directly populated through relaxation out of the FC point) drives the outcome of the excited state process, i.e. each specific SP typology ($SP_{anomalous}$ versus $SP_{standard}$) may determine different excited state paths and

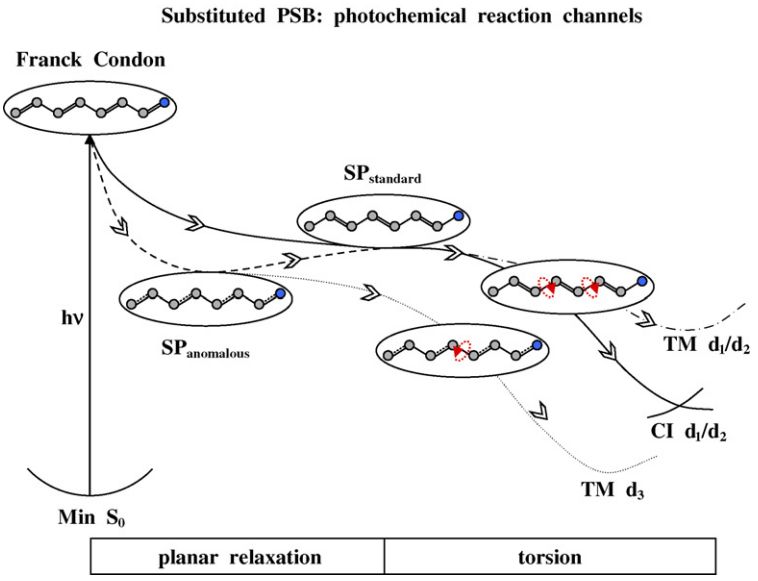


Scheme 4.

lead to a different photochemical reactivity. In fact, while qualitatively comparable relaxation paths as found in the parent compounds (i.e. isomerization of the internal stretched C=C double bonds) are expected from the standard SP structures, a different photochemical behavior (or, at least, a different energetic and efficiency) may occur from the anomalous points. These results suggest that substituents may also be used to tune the photochemical reactivity of these systems (not only the optical properties, as already seen in previous works [31]) and that, possibly, may play a role in the control of reaction selectivity/efficiency. We have shown above that this suggestion is indeed found. In particular, the photochemical reactivity of substituted-PSBs can be classified according to three different prototype behaviors (see Scheme 4):

(i) Substitution does not affect (both qualitatively and quantitatively) the photochemical behavior of the parent chromophore (see full lines in Scheme 4). Note that in these cases, initial relaxation leads to the standard planar stationary point ($SP_{standard}$). Fluorine-substituted system at C2 is an example belonging to this group. Thus, substitution may be only used in this case to tune the spectroscopic properties (absorption/emission).

(ii) Relaxation from the FC region leads to an anomalous planar stationary point ($SP_{anomalous}$) where double bond and single bond alternation is not jet inverted comparing to the Franck Condon structure. From this point, the chromophore accesses the same isomerization channels seen in the parent compound, although a very flat path or a tiny transition state is often involved (see dashed line in Scheme 4); furthermore, the twisted $S_1/S_0$ CI may be turned to a twisted minimum (TM $d_1/d_2$, dashed and dotted line in Scheme 4). This is the case for C4- and C6-fluorinated and C6-methoxylated systems. Alternatively, the twisting mode involves a barrierless OBF of the central single bond (see dotted line in Scheme 4), which ends into a twisted minimum on $S_1$ (TM $d_3$). This is a qualitatively different isomerization channel than those found in the parent system and it addresses a totally unusual photochemical behavior for PSB. C4 methoxy-substituted **2** belong to this group. Anyway, in all these cases photoisomerization rate and efficiency are expected to decrease, in general due to the flatness (or even the barrier) along the isomerization routes and/or the removal of the twisted conical intersection funnel, which may be replaced by a minimum.

(iii) A somehow intermediate case is represented by the $d_1$ isomerization for C3-fluorinated **2** and the $d_1$ and $d_2$ isomerization for C7-methoxylated **2**. Although a standard stationary point ($SP_{standard}$) is populated by the initial relaxation on $S_1$ and the following isomerization channels are qualitatively similar than those found in the parent system, a smaller photoisomerization rate and efficiency is expected since these paths may be very flat (mainly in the C7 methoxy-substituted case) and the twisted conical intersection funnel is replaced by a minimum (see the dashed and dotted line in Scheme 4).

## 5. Conclusions

We have provided ab initio state-of-the-art CASPT2//CASSCF computational clues that substitution may strongly affect the photo-reactivity of retinal chromophore models. In particular, we have shown that two different SP geometries may exist on the excited state according to the position of the substituent. Namely, C4 and C6-substituted systems display a stable anomalous SP point where the standard bond order alternation found in the other systems (including the unsubstituted parent compounds) is lacking and the bond alternation found in the FC geometry is substantially retained. Since this point is directly populated by relaxation out of the FC point (follow-

ing initial excitation), and it drives and control the following excited state dynamics leading to deactivation and photoisomerization, it is apparent that a substituent control of this structure (i.e. its stabilization) may be possibly used as a tool to tune photochemical reactivity and its efficiency/selectivity. Thus, the planar $S_1$ stationary point SP owns a fundamental rule in photoisomerization processes. If it is characterized by a C–C bonds inversion (i.e. double bonds becomes single and vice versa), the same reaction mechanism as for the parent unsubstituted compound is retained. On the other hand, if an anomalous SP appears (due to substituent stabilization) where double bonds are not stretched out, the photochemical reactivity could change either quantitatively (e.g. by decreasing only photoisomerization efficiency and selectivity) or even qualitatively (e.g. leading to different photochemical paths that yield a different photochemistry indeed). In conclusion, fluorine or methoxyl-substitution has the important role not only to tune the spectroscopic properties (absorption/emission) of the system, as seen in a previous work [31], but also to tune and even change the photochemical behavior of the PSB. Thus, this investigation together with the previous published work provides a full comprehensive analysis of substituent effects on the photochemical and photophysical properties of PSB chromophores.

To our knowledge this is the first computational study of this kind, which systematically investigate the effects of the substituents (namely fluorine and methoxyl) on the photochemical properties of retinal-PSB models. We think these results may be useful in molecular technology since they may provide a basis for the rational design of PSB-based photoswitchable devices and stimulate researches on the photochemistry of substituted retinal chromophores and their potential applications.

## Acknowledgments

This work has been supported in part by Funds for Selected Research Topics, MURST PRIN 2005 (project: "Trasferimenti di energia e di carica a livello molecolare") and FIRB (RBAU01L2HT).

## Appendix A. Valence bond analysis of MC-SCF wave functions

While the MEP provides a "structural" description of the isomerization process, detailed information on bond orders, electronic occupations and charge translocation has been obtained for $C_5H_6NH_2^+$ using concepts derived from valence bond (VB) theory. This VB approach to PSB photochemistry has been previously described (see ref. [18]). Briefly, the six bonding and anti-bonding it molecular orbitals, which result from a MC-SCF computation, are *localized* using the Boys localization procedure available in *Gaussian98*. [35] The resulting localized orbitals are just the six "p atomic orbitals" forming an atomic orbital (AO) basis of the π-system of the molecule. In this localized AO basis the CI expansion of the CAS wave function becomes a VB wave function consisting of covalent and ionic terms. The diagonal elements of the first-order density matrix (which we shall refer to as $D_{ii}$) and the elements of the spin exchange density matrix (which we shall refer to as $P_{ij}$) provide information on the occupancy of each AO and on the spin coupling (i.e. the *bonding* or *anti-bonding* status) between each pair ($ij$) of AO along the π-system, respectively. Since each AO resides on a different carbon or nitrogen centre of the $C_5H_6NH_2^+$ backbone, this information can be used to derive the valence bond resonance formulae that best describe the bonding status of the system. Specifically, the $P_{ij}$ have real values in the range between +1 and −1. A positive value close to +1 indicates that centre $i$ and $j$ are singlet spin coupled, i.e. *bonding*. In contrast a value between 0 and −1 indicates that the centres are either uncoupled, i.e. *non-bonding*, or triplet spin coupled (−1), i.e. *anti-bonding*. A more detailed discussion is given in ref. [18] and references cited therein.

In Fig. 6 we present the results of this wave function analysis at three relevant points (i.e. the FC point and the two SP minima) of $C_5H_6NH_2^+$. In the ground state structure of the FC point the positive $P_{ij}$ are located at the "formal" double bonds. The values of the diagonal elements of the first-order density matrix ($D_{ii}$) indicate that there is roughly one electron on each centre (with the exception of the C=N bond which is polarized towards the N atom so that $D_{ii}$ on the C atom is 0.7 and $D_{ii}$ on the N atom is 1.4). After the absorption of the photon the $P_{ij}$ at the C=N bond assumes a large and negative value and the terminal C=C $P_{ij}$ is strongly reduced in value. In contrast, the central C=C double bond remains substantially bonding. This bonding pattern explains the gradient direction on $S_1$, which corresponds to stretching of the C=N and terminal C=C bonds, in the initial part of the $S_1$ path. The large and positive $P_{ij}$ at the central double bond also indicates that at the FC geometry the system will be initially stable with respect to twisting motion *so that there is no tendency to initiate the cis → trans isomerization motion*. The $S_1$ electron density at the FC geometry shows a ∼0.5 electron increase on the C–N moiety and a corresponding decrease on the terminal C–C fragment. This is consistent with the charge transfer character of the $S_1$ state.

Interestingly, although the SP minima on $S_1$ do both describe a charge transfer state (see the $D_{ii}$ values), they are characterized by very different spin coupling terms ($P_{ij}$) along the π-system. It is clear from the $P_{ij}$ values that the standard SP structure ($SP_{standard}$) undergoes a dramatic change in bonding corresponding to a change from a *bonding* to an *anti-bonding* status of the central double bond. There is no dramatic change of the electron density, but rather simply a change in spin coupling. The new $P_{ij}$ pattern indicates that the force field of the central double bond is now very similar to that of a triplet coupling. Therefore, the system must be now *unstable* with respect to the central double bond twisting. This change in bonding explains the existence of an unstable central double bond and a barrierless isomerization reaction co-ordinate starting from $SP_{standard}$ (this change is summarized by the resonance structures given in Fig. 6). On the other hand, $P_{ij}$'s for the anomalous SP structure ($SP_{anomalous}$) reveal a different coupling for the central bond: a *bonding* status appears here, very similarly to FC (in fact, note that the $P_{ij}$ values found at the FC point are preserved in the anomalous SP structure). Thus, it is not surprising that from this point the

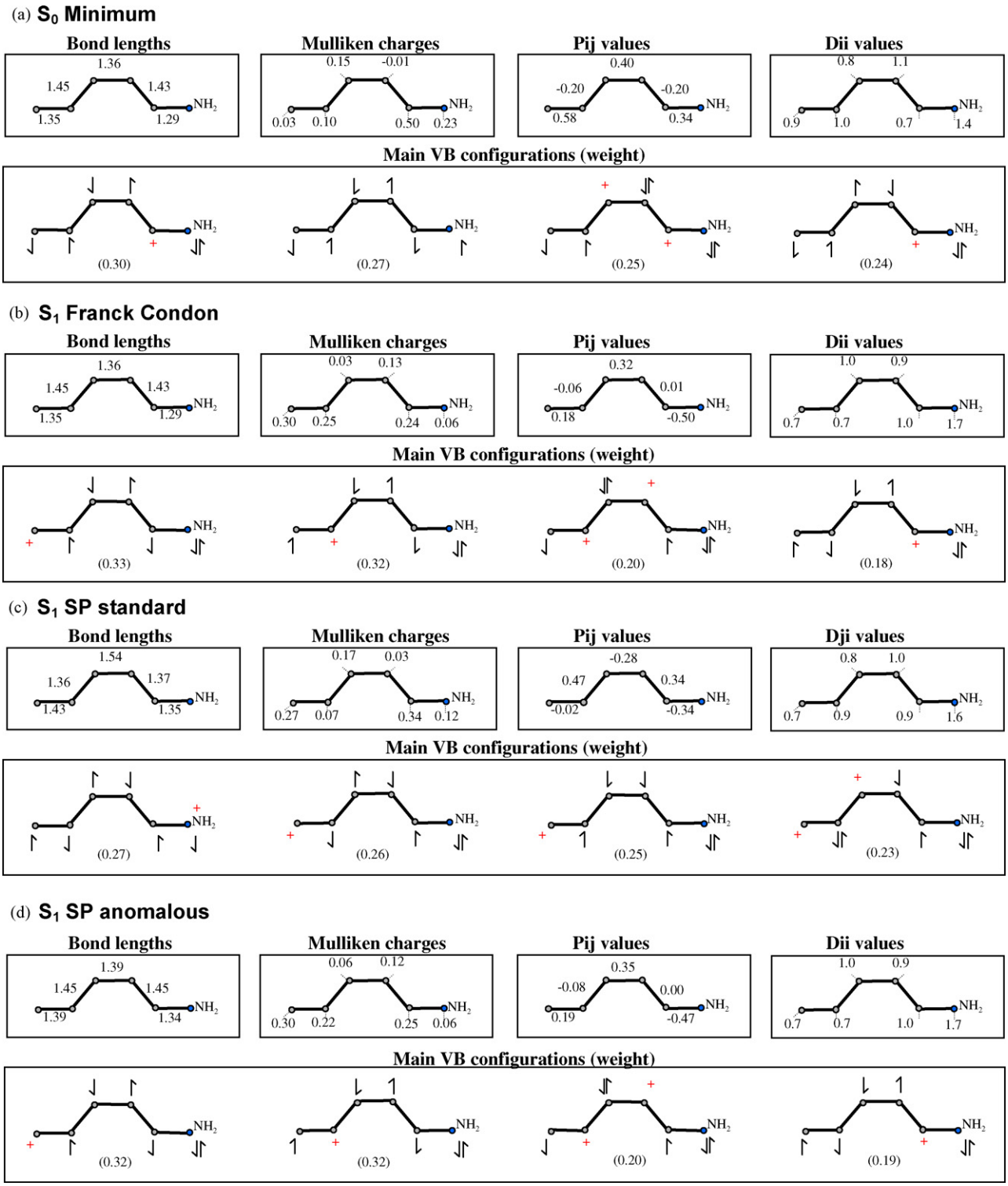


Fig. 6. *Pij*'s (spin exchange density matrix elements), *Dii*'s (diagonal elements of the first-order density matrix) and wave function Valente–Bond analysis at the FC (a and b), anomalous (c) and standard (d) SP points.

isomerization of the central bond is less favored (i.e. a barrier is likely involved) and/or different photochemical channels can be triggered.

In conclusion, VB analysis of the CASSCF wave function does show the existence on the charge transfer $S_1$ state of two different minima, which are characterized by a different bonding pattern of the $\pi$ electrons. In particular, while the single and double bonds are inverted at the $SP_{standard}$ point, the central bond preserves its double bond character at the $SP_{anomalous}$ point and its adjacent bonds are still single bonds.

## References


[1] G. Wald, Science 162 (1968) 230–239.
[2] R. Needleman, in: W.M. Horspool, P.-S. Song (Eds.), CRC Handbook of Organic Photochemistry and Photobiology, vol., CRC Press, Boca Raton, FL, 1995, pp. 1508–1515.
[3] M. Sugihara, J. Hufen, V. Buss, Biochemistry 45 (2006) 801–810.
[4] R. Vogel, F. Siebert, E.C.Y. Yan, T.P. Sakmar, A. Hirshfeld, M. Sheves, J. Am. Chem. Soc. 128 (2006) 10503–10512.
[5] H. Nakamichi, T. Okada, Proc. Natl. Acad. Sci. 103 (2006) 12729–12734.
[6] H. Kandori, Y. Shichida, T. Yoshizawa, Biochemistry (Moscow) 66 (2001) 1197–1209.
[7] R. Mathies, J. Lugtenburg, in: D.G. Stavenga, W.J. DeGrip, E.N.J. Pugh (Eds.), Molecular Mechanism of Vision, vol. 3, Elsevier Science Press, New York, 2000, pp. 55–90.
[8] A. Migani, A. Sinicropi, N. Ferré, A. Cembran, M. Garavelli, M. Olivucci, Faraday Discuss. 127 (2004) 179–191.
[9] K. Fujimoto, J.-Y. Hasegawa, S. Hayashi, S. Kato, H. Nakatsuji, Chem. Phys. Lett. 414 (2005) 239–242.
[10] T. Andruniow, N. Ferré, M. Olivucci, Proc. Natl. Acad. Sci. 101 (2004) 17908–17913.
[11] A. Cembran, R. Gonzáles-Luque, P. Altoè, M. Merchán, F. Bernardi, M. Olivucci, M. Garavelli, J. Phys. Chem. A 109 (2005) 6597–6605.
[12] M. Garavelli, T. Vreven, P. Celani, F. Bernardi, M.A. Robb, M. Olivucci, J. Am. Chem. Soc. 120 (1998) 1285–1288.
[13] A. Cembran, F. Bernardi, M. Olivucci, M. Garavelli, Proc. Natl. Acad. Sci. 102 (2005) 6255–6260.
[14] S. Sekharan, Weingart, V. Buss, Biophys. J. 91 (2006) L07–L09.
[15] A. Cembran, F. Bernardi, M. Olivucci, M. Garavelli, J. Am. Chem. Soc. 126 (2004) 16018–16037.
[16] R. González-Luque, M. Garavelli, F. Bernardi, M. Merchán, M.A. Robb, M. Olivucci, Proc. Natl. Acad. Sci. USA 97 (2000) 9379–9384.
[17] L. De Vico, C.S. Page, M. Garavelli, F. Bernardi, R. Basosi, M. Olivucci, J. Am. Chem. Soc. 124 (2002) 4124–4134.
[18] M. Garavelli, P. Celani, F. Bernardi, M.A. Robb, M. Olivucci, J. Am. Chem. Soc. 119 (1997) 6891–6901.
[19] M. Garavelli, F. Bernardi, M. Olivucci, T. Vreven, S. Klein, P. Celani, M.A. Robb, Faraday Discuss. 110 (1998) 51–70.
[20] L. De Vico, M. Garavelli, F. Bernardi, M. Olivucci, J. Am. Chem. Soc. 127 (2005) 2433–2442.
[21] A. Gilbert, J. Baggott, Essentials of Molecular Photochemistry, Blackwell Science, Oxford, 1991.
[22] N.J. Turro, Modern Molecular Photochemistry, Benjamin–Cummings, Menlo Park, CA, 1991.
[23] P. Hamm, M. Zurek, T. Roschinger, H. Patzelt, D. Oesterhelt, W. Zinth, Chem. Phys. Lett. 263 (1996) 613–621.
[24] H. Kandori, H. Sasabe, K. Nakanishi, T. Yoshizawa, T. Mizukami, Y. Shichida, J. Am. Chem. Soc. 118 (1996) 1002–1005.
[25] R.W. Schoenlein, L.A. Peteanu, R.A. Mathies, C.V. Shank, Science 254 (1991) 412–415.
[26] R.A. Mathies, C.H.B. Cruz, W.T. Pollard, C.V. Shank, Science 240 (1988) 777–779.
[27] H.J.A. Dartnall, Vision Res. 8 (1968) 339–358.
[28] T.J. Martinez, Accounts Chem. Res. 39 (2006) 119–126.
[29] A. Francesch, R. Alvarez, S. Lopez, A.R. De Lera, J. Org. Chem. 62 (1997) 310–319.
[30] A. Albeck, N. Friedman, M. Sheves, M. Ottolenghi, Biophys. J. 56 (1989) 1259–1265.
[31] I. Conti, F. Bernardi, G. Orlandi, M. Garavelli, Mol. Phys. 104 (2006) 915–924.
[32] P. Celani, M.A. Robb, M. Garavelli, F. Bernardi, M. Olivucci, Chem. Phys. Lett. 243 (1995) 1–8.
[33] M.J. Bearpark, M.A. Robb, H. Bernhard Schlegel, Chem. Phys. Lett. 223 (1994) 269–274.
[34] K. Andersson, M. Barysz, A. Bernhardsson, M.R.A. Blomberg, D.L. Cooper, M.P. Fülscher, C.D. Graaf, B.A. Hess, G. Karlström, R. Lindh, P.-Å. Malmqvist, T. Nakajima, P. Neogrády, J. Olsen, B.O. Roos, B. Schimmelpfennig, M. Schütz, L. Seijo, L. Serrano-Andrés, P.E.M. Siegbahn, J. Stålring, T. Thorsteinsson, V. Veryazov, P.-O. Widmark, MOLCAS, Version 5.4, Lund University, Sweden, 2002.
[35] M.J. Frisch, G.W. Trucks, H.B. Schlegel, G.E. Scuseria, M.A. Robb, J.R. Cheeseman, V.G. Zakrzewski, J.A.J. Montgomery, R.E. Stratmann, J.C. Burant, S. Dapprich, J.M. Millam, A.D. Daniels, K.N. Kudin, M.C. Strain, O. Farkas, J. Tomasi, V. Barone, M. Cossi, R. Cammi, B. Mennucci, C. Pomelli, C. Adamo, S. Clifford, J. Ochterski, G.A. Petersson, P.Y. Ayala, Q. Cui, K. Morokuma, D.K. Malick, A.D. Rabuck, K. Raghavachari, J.B. Foresman, J. Cioslowski, J.V. Ortiz, A.G. Baboul, B.B. Stefanov, G. Liu, A. Liashenko, P. Piskorz, I. Komaromi, R. Gomperts, R.L. Martin, D.J. Fox, T. Keith, M.A. Al-Laham, C.Y. Peng, A. Nanayakkara, C. Gonzalez, M. Challacombe, P.M.W. Gill, B. Johnson, W. Chen, M.W. Wong, J.L. Andres, C. Gonzalez, M. Head-Gordon, E.S. Replogle, J.A. Pople, Gaussian 98, Revision A.7, Gaussian, Inc., Pittsburgh PA, 1998.